

[Article]

doi: 10.3866/PKU.WHXB201901002

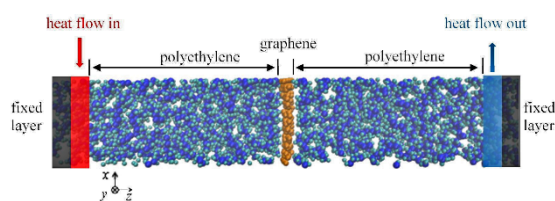
www.whxb.pku.edu.cn

## Toward Improved Thermal Conductance of Graphene-Polyethylene Composites *via* Surface Defect Engineering: A Molecular Dynamics Study

 XIONG Yangheng<sup>1</sup>, WU Hao<sup>1</sup>, GAO Jianshu<sup>1</sup>, CHEN Wen<sup>1</sup>, ZHANG Jingchao<sup>2,\*</sup>, YUE Yanan<sup>1,\*</sup>
<sup>1</sup> Key Laboratory of Hydraulic Machinery Transients (MOE), School of Power and Mechanical Engineering, Wuhan University, Wuhan 430072, P. R. China.

<sup>2</sup> Holland Computing Center, University of Nebraska-Lincoln, Lincoln, NE 68588, USA.

**Abstract:** Polymers are widely used advanced materials composed of macromolecular chains, which can be found in materials used in our daily life. Polymer materials have been employed in many energy and electronic applications such as energy harvesting devices, energy storage devices, light emitting and sensing devices, and flexible energy and electronic devices. The microscopic morphologies and electrical properties of the polymer materials can be tuned by molecular engineering, which could improve the device performances in terms of both the energy conversion efficiency and stability. Traditional polymers are usually considered to be thermal insulators owing to their amorphous molecular chains. Graphene-based polymeric materials have garnered significant attention due to the excellent thermal conductivity of graphene. Advanced polymeric composites with high thermal conductivity exhibit great potential in many applications. Therefore, research on the thermal transport behaviors in graphene-based nanocomposites becomes critical. Vacancy defects in graphene are commonly observed during its fabrication. In this work, the effects of vacancy defects in graphene on thermal transport properties of the graphene-polyethylene nanocomposite are comprehensively investigated using molecular dynamics (MD) simulation. Based on the non-equilibrium molecular dynamics (NEMD) method, the interfacial thermal conductance and the overall thermal conductance of the nanocomposite are taken into consideration simultaneously. It is found that vacancy defects in graphene facilitate the interfacial thermal conductance between graphene and polyethylene. By removing various proportions of carbon atoms in pristine graphene, the density of vacancy defects varies from 0% to 20% and the interfacial thermal conductance increases from 75.6 MW·m<sup>-2</sup>·K<sup>-1</sup> to 85.9 MW·m<sup>-2</sup>·K<sup>-1</sup>. The distinct enhancement in the interfacial thermal transport is attributed to the enhanced thermal coupling between graphene and polyethylene. A higher number of broken sp<sup>2</sup> bonds in the defective graphene lead to a decrease in the structure rigidity with more low-frequency (< 15 THz) phonons. The improved overlap of vibrational density states between graphene and polyethylene at a low frequency results in better interfacial thermal conductance. Moreover, the increase in the interfacial thermal conductance induced by vacancy defects have a significant effect on the overall thermal conductance (from 40.8 MW·m<sup>-2</sup>·K<sup>-1</sup> to 45.6 MW·m<sup>-2</sup>·K<sup>-1</sup>). In addition, when filled with the graphene layer, the local density of polyethylene increases on both sides of the graphene. The concentrated layers provide more aligned molecular arrangement, which result in better thermal conductance in polyethylene. Further, the higher local density of the polymer near the interface provides more atoms for interaction with the graphene, which leads to stronger effective interactions. The relative concentration is insensitive to the density of vacancy defects. The reported results on the thermal transport behavior of graphene-polyethylene composites provide reasonable guidance for using graphene as fillers to tune the thermal conduction of polymeric composites.



**Key Words:** Graphene; Polymeric composites; Thermal conductance; Vacancy defect; Molecular dynamics simulation

Received: January 2, 2019; Revised: January 21, 2019; Accepted: February 3, 2019; Published online: February 21, 2019.

\*Corresponding authors. Email: zhang@unl.edu; Tel: +01-402-909-5399 (J.Z.). Email: yyue@whu.edu.cn; Tel: +86-27-68772268 (Y.Y.).

The project was supported by the National Natural Science Foundation of China (51576145).

国家自然科学基金(51576145)资助项目

# 参杂缺陷石墨烯的高分子复合材料导热特性分子动力学模拟

熊扬恒<sup>1</sup>, 吴昊<sup>1</sup>, 高建树<sup>1</sup>, 陈文<sup>1</sup>, 张景超<sup>2,\*</sup>, 岳亚楠<sup>1,\*</sup>

<sup>1</sup> 武汉大学动力与机械学院水力机械过渡过程教育部重点实验室, 武汉 430072

<sup>2</sup> Holland Computing Center, 内布拉斯加大学林肯分校, 美国 林肯 68588

**摘要:** 传统高分子材料由于内部分子链无规则缠绕的特点, 导致其热导率较小。近年来, 拥有高导热特性的新型高分子材料在众多领域都显示出了极大的发展潜力。随着研究的不断深入, 具有优秀导热能力的石墨烯等低维碳材料引起越来越多人的关注。引入石墨烯制作的高分子复合材料具有较高的导热性能, 在热管理方面具有很大的应用前景。本文使用非平衡态分子动力学方法计算了石墨烯点缺陷对石墨烯-高分子复合材料界面热导和整体热导率的影响。石墨烯层的界面热导受点缺陷密度的影响较大。当石墨烯缺陷密度由0%增大到20%时, 其界面热导由 $75.6 \text{ MW}\cdot\text{m}^{-2}\cdot\text{K}^{-1}$ 增加为 $85.9 \text{ MW}\cdot\text{m}^{-2}\cdot\text{K}^{-1}$ 。石墨烯点缺陷造成 $sp^2$ 共价键断裂、结构刚性下降, 导致其振动态密度的低频分量增加, 增强了与高分子基质间的低频能量耦合, 进而提高了界面热导。而点缺陷密度的增大对复合材料整体热导率也具有相似的提升效果(从 $40.8 \text{ MW}\cdot\text{m}^{-2}\cdot\text{K}^{-1}$ 增加为 $45.6 \text{ MW}\cdot\text{m}^{-2}\cdot\text{K}^{-1}$ )。此外, 高分子基体在石墨烯界面处会造成局部密度提高, 但石墨烯点缺陷对高分子材料局部密度提升并无显著影响。这些计算结果加深了对石墨烯与高分子基体间导热机理的理解, 并有助于开发和设计具有优异热学性能的高分子复合材料。

**关键词:** 石墨烯; 高分子复合材料; 热导; 点缺陷; 分子动力学

**中图分类号:** O642

## 1 Introduction

In the past decade, lots of attentions have been given to the advanced polymer-based materials in applications such as fuel cells, wearable devices, and 3D printing<sup>1-3</sup>. However, the thermal conductivity of polymers is generally in the order of 0.1 to  $1 \text{ W}\cdot\text{m}^{-1}\cdot\text{K}^{-1}$  due to the amorphous arrangement of the molecular chains<sup>4-6</sup>. By changing the intrinsic structures of polymers through stretching, grafting and aligning *etc.*, numerous polymers with enhanced thermal conductivities have been reported<sup>7-10</sup>. Different from direct modifications of intrinsic structures, various thermally conductive fillers, including carbon fibers, carbon nanotubes (CNTs), graphene, ceramic and metal, have been introduced to enhance the thermal properties of polymers<sup>11-13</sup>. For example, Xu *et al.* investigated the thermal properties of composites with different single-walled carbon nanotube (SWNT) volume fractions. The highest thermal conductivity was increased by 130% at 49% (volume fraction) SWNT<sup>11</sup>.

Recently, graphene-based composite materials have garnered enormous attentions due to the superior thermal conductivity of graphene<sup>14-17</sup>. Adding graphene/graphite into pure polymer is expected to improve the thermal transport in the polymer composite<sup>18-20</sup>. Moreover, graphene and graphite are more cost-effective in practical fabrications compared to CNTs. Shahil *et al.* synthesized multilayer graphene-based composites as highly efficient thermal interface material which could enhance the heat transfer between two solid surfaces. An enhanced thermal conductivity of  $5 \text{ W}\cdot\text{m}^{-1}\cdot\text{K}^{-1}$  was achieved for the graphene-based polymer at a filler loading fraction of 10% (volume fraction)<sup>21</sup>. Kim *et al.* developed a fabrication method to allow

nanofillers with different shapes and sizes to evenly disperse in polymers. The thermal conductivity of graphene-resin composite was experimentally measured as  $0.87 \text{ W}\cdot\text{m}^{-1}\cdot\text{K}^{-1}$  at a mass fraction of 20%<sup>22</sup>. Shtein *et al.* reported a polymer matrix (epoxy) with an ultra-high thermal conductivity of  $12.4 \text{ W}\cdot\text{m}^{-1}\cdot\text{K}^{-1}$  at a filling fraction of 24% (volume fraction) graphene nanoplatelets. The remarkable improvement of thermal conductivity is mainly due to the closure of gaps between adjacent graphene nanoplatelets of large lateral dimensions and the low defect density<sup>23</sup>. Discrepancies among the experimental values are associated with different graphene morphology, volume fraction, polymeric material and measurement method<sup>24-26</sup>.

The perfect planar structure leads to the superior thermal conductivity in graphene. However, structural defects, such as single point vacancy, Stone-Wales defect, grain boundary, isotope doping and functionalization, are inevitable during the process of graphene fabrication and sample preparation<sup>27-29</sup>. Prior works have investigated the effect of the defect on thermal transport in graphene<sup>30-32</sup>. It is known that the introduced defects will suppress the thermal transport in graphene<sup>33-35</sup>. For example, a 7.5% of vacancy defects in graphene can reduce its thermal conductivity by nearly 300 times compared to that of pristine graphene<sup>34</sup>. Such a drastic reduction is attributed to the reduction of the mean free path and relaxation time of phonons within the defected graphene. The inner vacancy defect causes a stronger influence on the thermal conductance of graphene comparing to the edge vacancy defect effect<sup>36</sup>. However, the heat-transfer mechanism in graphene-based nanocomposites is unclear and remains an open topic.

In this work, the interfacial thermal conductance and the

overall thermal conductance of graphene-polyethylene composites is comprehensively studied using MD simulation. Based on the NEMD method, the effect of vacancy defect with different densities is explored. The interfacial thermal conductance between the sandwiched graphene layer and the polymeric material and the overall thermal conductance in the nanocomposite are investigated respectively. Moreover, frequency domain analysis is carried out to explain the mechanism of interfacial energy transport. The structure concentration effect of polymeric materials is observed when a graphene layer is embedded in the nanocomposites. Our simulation utilizes an effective approach for thermal analysis in small-scale nanocomposites, and the calculated results provide valuable guidance for using defective graphene as fillers to tune the thermal conduction in polymeric composites.

## 2 Methods and simulations

The polymeric material used in this work is polyethylene ( $C_{20}H_{42}$ ). As shown in Fig. 1a, the graphene-polyethylene composite consists of two amorphous polyethylene blocks and a sandwiched graphene layer. The structure is designed with an overall length of 12 nm and a cross-sectional area of  $2 \text{ nm} \times 2 \text{ nm}$ . All simulations are carried out using the LAMMPS package with a time step of  $0.25 \text{ fs}$ <sup>37</sup>.

The adaptive intermolecular reactive empirical bond order (AIREBO) potential<sup>38</sup>, which has been widely used in simulations of carbon systems<sup>39</sup>, is used to model the graphene layer. The condensed-phase optimized molecular potential for atomistic simulation studies (COMPASS) is used to model the polymer molecules<sup>40</sup>. The COMPASS potential has been employed to study the thermal energy transport in polymeric materials, and the calculated thermal conductivities are found to match well with the experimental results<sup>41</sup>. The interactions

between the graphene and polyethylene (van der Waals interactions) are modeled by Lenard-Jones (LJ) potential, which is described as

$$V(r) = 4\epsilon_0[(\sigma_0/r)^{12} - (\sigma_0/r)^6] \quad (1)$$

where  $\epsilon_0$  is the energy parameter,  $r$  is the interatomic distance and  $\sigma_0$  is the van der Waals diameter. The LJ parameters used in this work are shown in Table 1. It has been proved that the specific parameters in Table 1 are applicable in describing the mechanical properties of graphene and polyethylene model<sup>42</sup>.

The NEMD method is employed to calculate the thermal transport in graphene-polyethylene composites<sup>43</sup>. Periodic boundary conditions are applied in  $x$  and  $y$  directions. After energy minimization, the simulation domain in the  $z$ -direction is extended 2 nm larger than the original dimension to avoid the possible interaction between the two ends. The system is initially equilibrated at temperature 300 K for 500 ps in thermal-isobaric ensemble ( $NPT$ ). A micro-canonical ensemble ( $NVE$ ) is followed for another 250 ps. Atoms (1 nm) at both ends of the sample are fixed to stabilize the free edge. Two adjacent layers of 0.8 nm are grouped as heat source and sink in Fig. 1a, respectively. A constant heat flux rate  $\dot{q}$  is applied to the system for 1500 ps in  $NVE$  ensemble to ensure the temperature gradient reaches steady state. The steady-state temperature profile is presented in Fig. 1b. There is a temperature jump  $\Delta T$  at the interface between graphene and polyethylene. Then the interfacial thermal conductance can be calculated as  $G = \dot{q} / \Delta T$ , where  $\Delta T$  is obtained by averaging the data over a period of 500 ps in steady state.

## 3 Results and discussion

### 3.1 Effect of defect on interfacial thermal transport

Prior works have investigated the effect of defect on thermal transport in graphene<sup>30</sup>. Aside from in-plane thermal transport, vacancy defect affects the interfacial thermal conductance of graphene embedded in polymeric materials as well. In our simulation, we explored the effect of defects on interfacial thermal transport by removing various numbers of carbon atoms (4 to 32) from the center of single-layer graphene. With 160 atoms in the graphene sheet, the density of defects ranges from 0 to 20%.

In our thermal transport model, heat flows across the embedded graphene layer and develops a steady-state temperature gradient (shown in Fig. 1b). The interfacial thermal conductance is determined to be  $75.6 \pm 1.9 \text{ MW} \cdot \text{m}^{-2} \cdot \text{K}^{-1}$ , which is very close to the reported value for single layer graphene embedded in polymeric materials<sup>44-46</sup>. As shown in Fig. 2, the thermal conductance of the graphene layer has a positive

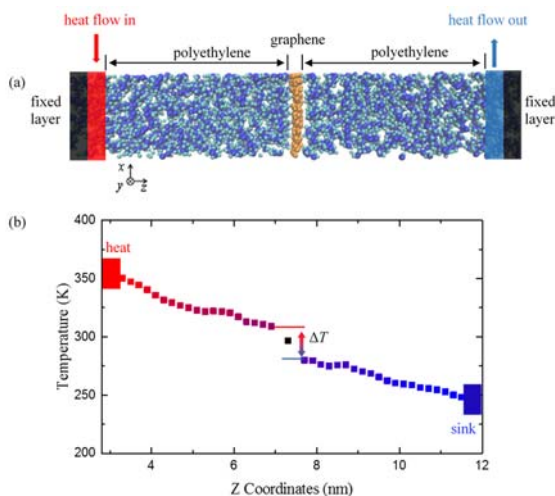


**Fig. 1** (a) Graphene-polyethylene composite in NEMD simulation. (b) The steady-state temperature profile along the heat flux direction.

Graphene is set as the embedded layer in the middle of polyethylene. Heat flow runs across the composite with the fixed layer setting at the end of the system. The  $\Delta T$  represents the temperature drop at the interface between graphene and polyethylene.

**Table 1** Lenard-Jones parameters of different atom types.

Atom	Energy constant $\epsilon$ (eV)	Distance constant $\sigma$ (nm)
carbon (in graphene)	0.002390	0.3412
carbon (in polyethylene)	0.002341	0.4010
hydrogen	0.000867	0.2995

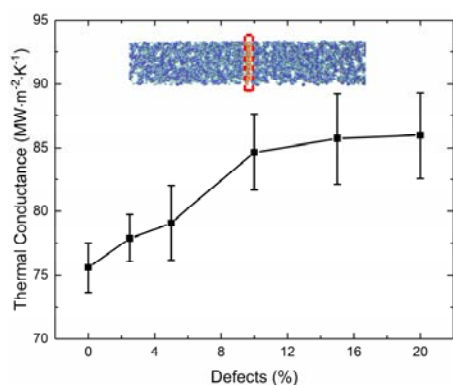


**Fig. 2 Interfacial thermal conductance as a function of vacancy defects. Insert schematics show the interfacial area.**

correlation with the density of vacancy defects. With increasing defect concentrations from 0% to 20%, the thermal conductance increases from  $75.6 \text{ MW}\cdot\text{m}^{-2}\cdot\text{K}^{-1}$  to  $85.9 \text{ MW}\cdot\text{m}^{-2}\cdot\text{K}^{-1}$ . Previous MD simulation showed that a 4.17% defect in graphene has a negligible effect on the graphene-paraffin interfacial thermal transport<sup>42</sup>. Compared to the reference data, the thermal conductance increases marginally ( $\sim 14\%$ ) with higher defect concentrations in our simulation results.

To understand the evolution of interfacial thermal conductance, the vibrational density of states (VDOS) is employed to characterize the energy of atomic vibrations. It is calculated by taking the fast Fourier transform (FFT) of the velocity autocorrelation function of atoms. The VDOS in frequency domain is given by

$$P(\omega) = \int_0^t \langle v(t)v(0) \rangle \exp(-i\omega t) dt \quad (2)$$

where  $\omega$  is frequency,  $v(0)$  and  $v(t)$  are atomic velocities at the initial time and at time  $t$ , respectively. Fig. 3 shows the VDOS spectra of polyethylene and graphene. The poor spectra overlap between graphene and polyethylene leads to an ineffective interfacial thermal conductance. It is noted that the out-of-plane VDOS at low-frequencies (less than 15 THz) make the most contributions to the overlap between the pristine graphene and the polyethylene, which is in agreement with prior studies<sup>47</sup>. The VDOS spectra of graphene under three defects concentrations (0%, 10%, 20%) are shown in Fig. 3a. With more defects on the graphene layer, the low-frequency vibration modes of graphene are increased, promoting the interfacial thermal coupling between graphene and surrounding polyethylene. This evolution of low-frequency vibration modes is caused by the loss of  $sp^2$  bonds in graphene<sup>48</sup>. The number of covalent bonds is reduced in graphene when vacancy defects are introduced. Therefore, the embedded graphene layer in the composite becomes less rigid structurally which leads to an increase of low-frequency vibration modes. Consequently, the interfacial thermal transport is enhanced due to the existing of vacancy defects in graphene.

### 3.2 Effect of defect on overall thermal conductance

By utilized the same simulation model in Fig. 1a, the effect of vacancy defect on the thermal performance of nanocomposites

is investigated. To quantitatively evaluate the effect of vacancy defect on the overall thermal conductance of graphene-polyethylene composites, an area of  $2 \text{ nm} \times 2 \text{ nm} \times 2.8 \text{ nm}$  is selected, which contains graphene atoms and a consistent volume of polyethylene as shown in Fig. 4a.

To remain consistent with previous calculations, the same heat flux is imposed on the nanocomposites. The corresponding temperature drop  $\Delta T$  is shown in Fig. 4b. The overall thermal conductance can be also calculated as  $G = q/\Delta T$ .

As shown in Fig. 5, as the density increases from 0% to 20%, the thermal conductance increases from  $40.8 \text{ MW}\cdot\text{m}^{-2}\cdot\text{K}^{-1}$  to  $45.6 \text{ MW}\cdot\text{m}^{-2}\cdot\text{K}^{-1}$ . The vacancy defect has a relatively smaller effect on the overall thermal conductance when compared to the effect on the interfacial thermal conductance. In consideration of our small evaluation area, the increase of interfacial thermal

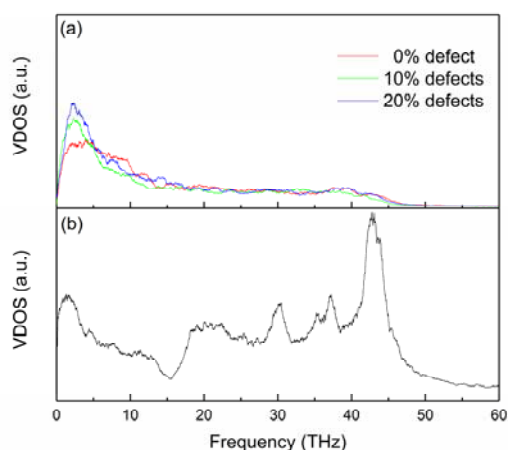


**Fig. 3 (a) Out-of-plane VDOS spectra at three defect concentrations (0%, 10% and 20%). (b) VDOS spectra of polyethylene.**

The VDOS spectra are the averaged results for corresponding graphene and polyethylene atoms.

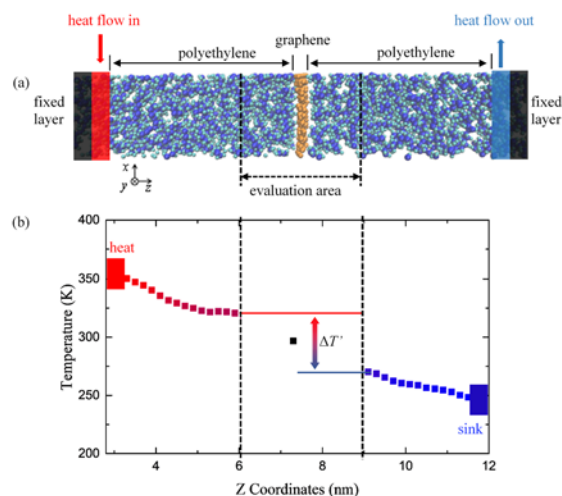


**Fig. 4 (a) Schematic of the simulation model for overall thermal conductance evaluation. (b) The steady-state temperature profile of the composite along the heat flow direction.**

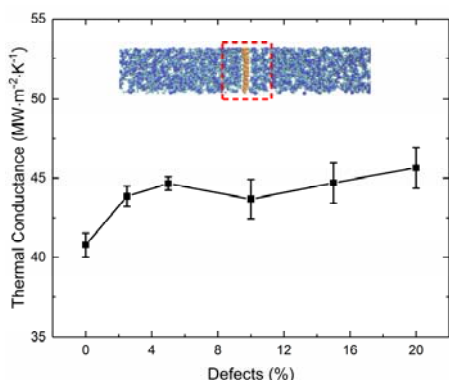


**Fig. 5** Overall thermal conductance of the evaluation area as a function of vacancy defects. Insert figure shows the evaluation area.

conductance induced by vacancy defect has a significant effect on the overall thermal conductance. Moreover, as the size of graphene increases, the interfacial thermal transport has less influences on the overall thermal conductance of nanocomposites<sup>48</sup>.

More than the effect of interfacial thermal transport, the distribution of the molecular chains could also affect the overall thermal conductance in the nanocomposite. Fig. 6 shows the relative concentration of nanocomposite and polyethylene along the heat flow direction. The horizontal axis is the distance from the central graphene layer. The peak density at 0 nm is the relative concentration of carbon atoms in graphene. The black line represents the relative concentration of pure polyethylene model. It is indicated that the polyethylene molecules are uniformly distributed with no stratification or concentration. However, when a graphene layer is sandwiched within the polyethylene, the density distribution of the molecular chains exhibits sinusoidal fluctuations. The distance between graphene and the adjacent polyethylene is about 0.17 nm which is half the thickness of graphene<sup>49</sup>.

It is observed that the density of polyethylene increases near the interface and falls back to the normal level with growing distance from the graphene layer. The concentrated layers of polyethylene have aligned molecular arrangement<sup>50</sup>, which results in a better thermal conductivity in polymeric materials<sup>10</sup>.

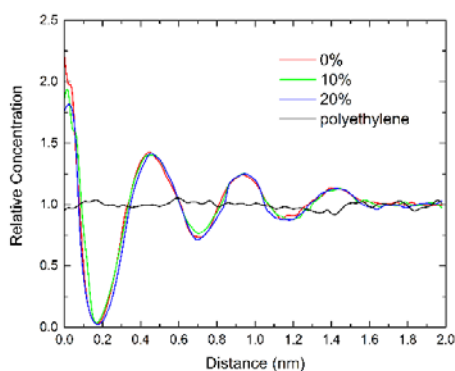


**Fig. 6** Relative concentration of nanocomposite and polyethylene along the heat flow direction.

Two main concentrated layers of polyethylene are at distances of 0.45 and 0.95 nm with relative peak concentration of 50% and 25%, respectively. The fading peak concentration and widening peak width in Fig. 6 indicate a decreasing interaction between graphene and polyethylene. It is found that thermal transport across graphene-polymer interface can be enhanced by increasing the polymer density. Luo *et al.*<sup>45</sup> explained this density effect using VDOS analyses: the shorter interatomic distances lead to stronger van der Waals forces and greater overlaps between the spectra of polymer and graphene which results in better interfacial thermal coupling. Besides, the higher local density of polymer near the interface provides more atoms for interacting with graphene, which directly facilitates the interfacial thermal conductance.

## 4 Conclusions

To sum up, the interfacial thermal conductance and the overall thermal conductance of the graphene-polyethylene composites are comprehensively investigated using NEMD method. With increasing density of vacancy defect from 0% to 20% in graphene, the interfacial thermal conductance increases from 75.6 MW·m<sup>-2</sup>·K<sup>-1</sup> to 85.9 MW·m<sup>-2</sup>·K<sup>-1</sup>. The calculated interfacial thermal conductance increases with defect concentrations due to the increased populations of low frequency phonons, which results in better VDOS overlaps between graphene and polyethylene. Meanwhile it is found that vacancy defects have relatively smaller effect on the overall thermal conductance (from 40.8 MW·m<sup>-2</sup>·K<sup>-1</sup> to 45.6 MW·m<sup>-2</sup>·K<sup>-1</sup>). It is reported that the local structure with higher density of polyethylene near the interface provides more atoms for interacting with graphene. Our results indicate that the thermal performance of polymeric composites can be effectively tuned *via* surface engineering of graphene and provide guidance for future development of graphene-based composites for practical thermal applications.

## References

- (1) Sun, Y.; Shi, G. *J. Polym. Sci. B. Polym. Phys.* **2013**, *51* (4), 231. doi: 10.1002/polb.23226
- (2) Wang, Y.; Chen, K. S.; Mishler, J.; Cho, S. C.; Adroher, X. C. *Appl. Energy* **2011**, *88* (4), 981. doi: 10.1016/j.apenergy.2010.09.030
- (3) Zarek, M.; Layani, M.; Cooperstein, I.; Sacyani, E.; Cohn, D.; Magdassi, S. *Adv. Mater.* **2016**, *28* (22), 4449. doi: 10.1002/adma.201503132
- (4) Henry, A. *Annu. Rev. Heat Transfer* **2013**, *17*, 485. doi: 10.1615/AnnualRevHeatTransfer.2013006949
- (5) Choy, C. *Polymer* **1977**, *18* (10), 984. doi: 10.1016/0032-3861(77)90002-7
- (6) Wang, X.; Zhang, J.; Chen, Y.; Chan, P. K. L. *Nanoscale* **2017**, *9* (6), 2262. doi: 10.1039/c6nr08682a
- (7) Poulaert, B.; Legras, R.; Chielens, J.; Vandenhende, C.; Issi, J. *Polym.*



- Commun.* **1990**, *31* (4), 148.  
doi: 10.1016/0032-3861(78)90032-0
- (8) Shen, S.; Henry, A.; Tong, J.; Zheng, R.; Chen, G. *Nat. Nanotechnol.* **2010**, *5* (4), 251. doi: 10.1038/nano.2010.27
- (9) Xu, Y.; Wang, X.; Zhou, J.; Song, B.; Jiang, Z.; Lee, E. M.; Huberman, S.; Gleason, K. K.; Chen, G. *Sci. Adv.* **2018**, *4* (3), eaar3031. doi: 10.1126/sciadv.aar3031
- (10) Singh, V.; Bougher, T. L.; Weathers, A.; Cai, Y.; Bi, K.; Pettes, M. T.; McMenamin, S. A.; Lv, W.; Resler, D. P.; Gattuso, T. R. *Nat. Nanotechnol.* **2014**, *9* (5), 384. doi: 10.1038/nano.2014.44
- (11) Xu, Y.; Ray, G.; Abdel-Magid, B. *Compos. Part A Appl. Sci. Manuf.* **2006**, *37* (1), 114. doi: 10.1016/j.compositesa.2005.04.009
- (12) Han, Z.; Fina, A. *Prog. Polym. Sci.* **2011**, *36* (7), 914. doi: 10.1016/j.progpolymsci.2010.11.004
- (13) Lee, G. -W.; Park, M.; Kim, J.; Lee, J. I.; Yoon, H. G. *Compos. Part A Appl. Sci. Manuf.* **2006**, *37* (5), 727. doi: 10.1016/j.compositesa.2005.07.006
- (14) Balandin, A. A.; Ghosh, S.; Bao, W.; Calizo, I.; Teweldebrhan, D.; Miao, F.; Lau, C. N. *Nano Lett.* **2008**, *8* (3), 902. doi: 10.1021/nl0731872
- (15) Ghosh, S.; Calizo, I.; Teweldebrhan, D.; Pokatilov, E. P.; Nika, D. L.; Balandin, A. A.; Bao, W.; Miao, F.; Lau, C. N. *Appl. Phys. Lett.* **2008**, *92* (15), 151911. doi: 10.1063/1.2907977
- (16) Hong, Y.; Ju, M. G.; Zhang, J.; Zeng, X. C. *Phys. Chem. Chem. Phys.* **2018**, *20* (4), 2637. doi: 10.1039/c7cp06874c
- (17) Hong, Y.; Zhang, Z.; Zhang, J.; Zeng, X. C. *Nanoscale* **2018**, *10* (40), 19092. doi: 10.1039/c8nr05703f
- (18) Zhang, L.; Bai, Z.; Liu, L. *Adv. Mater. Interfaces* **2016**, *3* (13), 1600211. doi: 10.1002/admi.201600211
- (19) Wang, X.; Zhang, J.; Chen, Y.; Chan, P. K. *Phys. Chem. Chem. Phys.* **2017**, *19* (24), 15933. doi: 10.1039/C7CP01958K
- (20) Han, D.; Wang, X. Y.; Ding, W. Y.; Chen, Y.; Zhang, J. C.; Xin, G. M.; Cheng, L. *Nanotechnology* **2019**, *30* (7), 075403. doi: 10.1088/1361-6528/aaf481
- (21) Shahil, K. M.; Balandin, A. A. *Nano Lett.* **2012**, *12* (2), 861. doi: 10.1021/nl203906r
- (22) Kim, S. Y.; Noh, Y. J.; Yu, J. *Compos. Part A Appl. Sci. Manuf.* **2015**, *69*, 219. doi: 10.1016/j.compositesa.2014.11.018
- (23) Shtein, M.; Nativ, R.; Buzaglo, M.; Kahil, K.; Regev, O. *Chem. Mater.* **2015**, *27* (6), 2100. doi: 10.1021/cm504550e
- (24) Wang, Y.; Zhan, H.; Xiang, Y.; Yang, C.; Wang, C. M.; Zhang, Y. J. *Phys. Chem. C* **2015**, *119* (22), 12731. doi: 10.1021/acs.jpcc.5b02920
- (25) Wang, T. -Y.; Tsai, J. -L. *Comput. Mater. Sci.* **2016**, *122*, 272. doi: 10.1016/j.commatsci.2016.05.039
- (26) Qu, W. D.; Liu, J.; Xue, Y.; Wang, X. W.; Bai, X. L. *J. Appl. Polym. Sci.* **2018**, *135* (4), 45736. doi: 10.1002/App.45736
- (27) Gass, M. H.; Bangert, U.; Bleloch, A. L.; Wang, P.; Nair, R. R.; Geim, A. *Nat. Nanotechnol.* **2008**, *3* (11), 676. doi: 10.1038/nnano.2008.280
- (28) Schniepp, H. C.; Li, J. -L.; McAllister, M. J.; Sai, H.; Herrera-Alonso, M.; Adamson, D. H.; Prud'homme, R. K.; Car, R.; Saville, D. A.; Aksay, I. A. *J. Phys. Chem. B* **2006**, *110* (17), 8535. doi: 10.1021/jp060936f
- (29) Tang, X.; Xu, S.; Zhang, J.; Wang, X. *ACS Appl. Mater. Interfaces* **2014**, *6* (4), 2809. doi: 10.1021/am405388a
- (30) Kotakoski, J.; Krashenninnikov, A.; Kaiser, U.; Meyer, J. *Phys. Rev. Lett.* **2011**, *106* (10), 105505. doi: 10.1103/PhysRevLett.106.105505
- (31) Hao, F.; Fang, D.; Xu, Z. *Appl. Phys. Lett.* **2011**, *99* (4), 041901. doi: 10.1063/1.3615290
- (32) Zhang, J.; Hong, Y.; Yue, Y. *J. Appl. Phys.* **2015**, *117* (13), 134307. doi: 10.1063/1.4916985
- (33) Chen, S.; Wu, Q.; Mishra, C.; Kang, J.; Zhang, H.; Cho, K.; Cai, W.; Balandin, A. A.; Ruoff, R. S. *Nat. Mater.* **2012**, *11* (3), 203. doi: 10.1038/nmat3207
- (34) Zhang, H.; Lee, G.; Cho, K. *Phys. Rev. B* **2011**, *84* (11), 115460. doi: 10.1103/PhysRevB.84.115460
- (35) Yue, Y.; Zhang, J.; Xie, Y.; Chen, W.; Wang, X. *Int. J. Heat Mass Transf.* **2017**, *110*, 827. doi: 10.1016/j.ijheatmasstransfer.2017.03.082
- (36) Jiang, J. -W.; Wang, B. -S.; Wang, J. -S. *Appl. Phys. Lett.* **2011**, *98* (11), 113114. doi: 10.1063/1.3567768
- (37) Plimpton, S. *J. Comput. Phys.* **1995**, *117* (1), 1. doi: 10.1006/jcph.1995.1039
- (38) Brenner, D. W.; Shenderova, O. A.; Harrison, J. A.; Stuart, S. J.; Ni, B.; Sinnott, S. B. *J. Phys. Condens. Matt.* **2002**, *14* (4), 783. doi: 10.1088/0953-8984/14/4/312
- (39) Hu, J.; Ruan, X.; Chen, Y. P. *Nano Lett.* **2009**, *9* (7), 2730. doi: 10.1021/nl901231s
- (40) Sun, H. *J. Phys. Chem. B* **1998**, *102* (38), 7338. doi: 10.1021/jp980939v
- (41) Liu, J.; Yang, R. *Phys. Rev. B* **2010**, *81* (17), 174122. doi: 10.1103/PhysRevB.81.174122
- (42) Wang, Y.; Yang, C.; Cheng, Y.; Zhang, Y. *RSC Adv.* **2015**, *5* (101), 82638. doi: 10.1039/C5RA12028D
- (43) Hoover, W. G. *Annu. Rev. Phys. Chem.* **1983**, *34* (1), 103. doi: 10.1146/annurev.pc.34.100183.000535
- (44) Shen, X.; Wang, Z.; Wu, Y.; Liu, X.; He, Y. -B.; Kim, J. -K. *Nano Lett.* **2016**, *16* (6), 3585. doi: 10.1021/acs.nanolett.6b00722
- (45) Luo, T.; Lloyd, J. R. *Adv. Funct. Mater.* **2012**, *22* (12), 2495. doi: 10.1002/adfm.201103048
- (46) Liu, Y.; Huang, J.; Yang, B.; Sumpter, B. G.; Qiao, R. *Carbon* **2014**, *75*, 169. doi: 10.1016/j.carbon.2014.03.050
- (47) Hu, L.; Desai, T.; Keblinski, P. *J. Appl. Phys.* **2011**, *110* (3), 033517.

doi: 10.1063/1.3610386

(48) Liu, Y.; Hu, C.; Huang, J.; Sumpter, B. G.; Qiao, R. *J. Chem. Phys.*

**2015**, *142* (24), 244703. doi: 10.1063/1.4922775

(49) Girifalco, L.; Hodak, M.; Lee, R. S. *Phys. Rev. B* **2000**, *62* (19),

13104. doi: 10.1103/PhysRevB.62.13104

(50) Chen, S.; Lv, Q.; Guo, J.; Wang, Z.; Sun, S.; Hu, S. *Acta Polym. Sin.*

**2017**, (4), 716. doi: 10.11777/j.issn1000-3304.2017.16201